RADIOMETRIC EQUALIZATION OF REMOTE SENSING DATA BY UTILIZATION OF LASERSCAN DATA

J. Bückner, M. Pahl, O. Stahlhut

Institut für Theoretische Nachrichtentechnik
und Informationsverarbeitung (TNT)
http://www.tnt.uni-hannover.de
University of Hannover, Germany
{bueckner, pahl, stahlhut, geoaida}@tnt.uni-hannover.de

ABSTRACT

This contribution describes a new approach for detection of shadow areas appearing in remote sensing image data. Identification of objects like streets or vehicles is frequently disturbed by illumination effects like hard shadows or inhomogenous darkening due to varying tilt angles of the processed terrain. To increase the reliability of the recognition process, we apply a sensor fusion of elevation data from laserscanning and optical image data. The represented algorithm improves the results iteratively. The different results are discussed and then used for further processing within a radiometric equalization.

1. INTRODUCTION

Environmental monitoring tasks based on remote sensing images, especially the update of geographic information data, become more and more important. Due to the increasing number of such images and the labour-intensive manual evaluation there is strong demand for productive and robust techniques for automatic analysis and object extraction.

Interferences in aerial images caused by shadows aggravate object recognition by image processing methods, e.g. road detection ([Baumgartner *et al.*, 1999], [Bückner, 1998]). Especially in the context of knowledge-based analysis ([Tönjes *et al.*, 1999], [Bückner *et al.*, 2000]), it is very important, to identify the shadow areas in the image data and use this information to control the analysis operation and the object recognition process. Furthermore it is possible to correct detected shadow areas by a radiometric equalization to improve the results of a consecutive object recognition.

This contribution shows the application of sensor data fusion for a shadow detection algorithm. Two example input images are shown in fig. 1. Precondition for this multi sensorial approach is the registration of all image data onto a common geocoordinate system. In addition to the aerial, optical images laserscan data is evaluated for height detection. The laserscan data which is used here as supplementary input will be one of the standard remote sensing sources in the near future, as it is used for creation of digital elevation models (DEM).

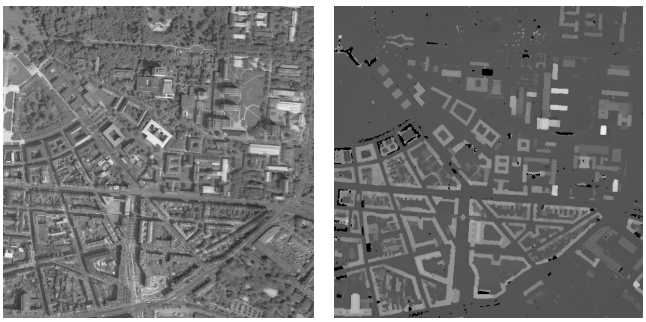

Fig. 1. Visual and laserscan image

The shadow regions are extracted according to the following steps. First, the buildings are automatically segmented in the elevation data. Their position is used for a rough estimate of the affiliated shadow regions. Further analysis of these preliminary shadow areas computes a threshold value which is used for binarisation of the whole visual input image. Despite of the simple approach this first step already delivers all the shadowed areas, but unfortunately also regions, which appear dark in the image due to their material properties.

In order to improve the results of step one, the position of the sun at the acquisition time of the visual image is calculated from the elevation model and the already determined shadow regions from step one. Using these parameters for a projection of the height model a second result can be calculated. Both results can be used as input to a radiometric equalization or as auxiliary data for a knowledge-based image interpretation.

In the first part (Sec. 2) of this contribution the data used for processing is described briefly. Afterwards, a *first* shadow image is created from the visual data by application of a threshold value. Using this result and the elevation data the position of the sun at the time of image acquisition is estimated (Sec. 3). A *second* shadow image is calculated in Sec. 4 by artificial illumination of the elevation model according to the sun position. The radiometric equalization in Sec. 5 uses a combination of both results.

2. SENSOR DATA

For the examination of the algorithms we present here, a visual data set and a digital elevation model (DEM) are used. The visual images have a resolution of 0.25m per pixel, the laserscan data resolution is 1m per pixel. The laserscan data acquired in autumn show the area without the vegetation heights. The visual images captured in summer however show leafy trees. Before the analysis both data records have be registered to a common geo coordinate system and the DEM is resampled to the resolution of the visual image. This offers direct correspondence of the different data sources on pixel level.

In a first step the buildings have to be extracted. Since altitude edges of house walls are well reproduced by the laserscan data, it is possible to use the position of these edges together with shape parameters to detect areas, that represent houses in the sensor data. To accomplish this task the altitude egdes are extracted from the laserscan data in the first step. In a second step regions, whose locale height differences are below a given threshold value are connected and filled with a uniform and unique label. Labelregions smaller than a minimum size, as they occur e.g. in forest areas, are assigned to the surrounding region, large regions exceeding a maximum size are assigned to the background. This segmentation process results in a label image, in which each building is represented by a random colour value (Fig. 2).

3. SHADOW DETECTION IN THE VISUAL IMAGE

The determination of a threshold to create a *first* shadow image is described now. The detected buildings are used, in order to determine the buildings' shadows. Starting orthogonal to the buildings' boundaries a four direction search for dark areas is initiated. Since this search starts at the buildings' boundaries and withdraws itself from them continuously, the end of the shadow can be determined by a hard transition of dark to bright pixel values, i.e. a distinct gradient. The sides of a building with no adjacent shadow area, can be differentiated from the shadow regions by their luminance values.

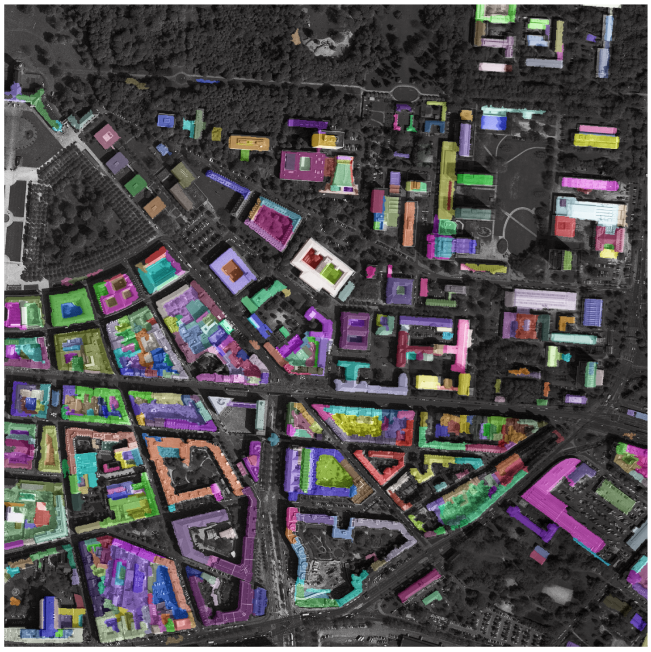

Fig. 2. Detected buildings

The pixels touched by this search can now be used for a histogram analysis, in order to determine a threshold value, which separates the whole visual image into shadowed and non-shadowed areas. Apart from the real shadow areas, falsely classified regions are produced, which appear dark due to their material properties within the visual image. This intermediate result serves as base for the following steps, which are insensitive to the observed errors. A small part of the result image is shown in figure 4.

4. SHADOW PROJECTION

Now the DEM is used to calculate a second shadow picture. On the basis of the previous result and the available height data the remaining errors are eliminated now. For this the elevation model derived from the laserscan data is illuminated with an artificial sun positioned according to the recording time of the visual data. Since this elevation model represents the object heights, the resulting shadow image does not contain the errors, which occurred during the threshold value search described above.

4.1. Determination of the position of the sun

If the image recording time (place, date, time-of-day) is available, the position of the sun can be derived directly from this information. Since these parameters are not always present, we now describe, how the position of the sun at the image recording time is determined using the already available *first* shadow image and the height data.

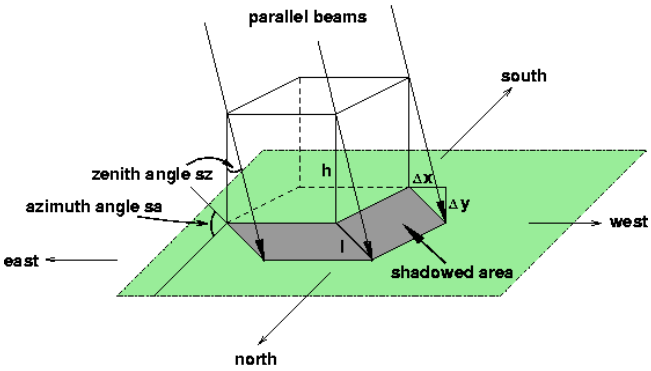

Fig. 3. Position of the azimuth and zenith angle

Figure 3 shows the height data as well as the shadow areas. The azimuth angle can be calculated from the shadow length, the zenith angle using the height of the building. These relations are shown in equation 1 and equation 2.

$$\tan(\alpha) = \frac{\Delta y}{\Delta x} \longrightarrow sa = 90° + \alpha \tag{1}$$

$$\tan(\beta) = \frac{h}{l} \longrightarrow sz = 90° - \beta \tag{2}$$

In order to determine the two angles, the corners of the houses in the height data and the corresponding corners in the shadow image must be detected. The buildings' corners can be extracted from the label image (figure 2) mentioned above. Starting from these positions the corners of the corresponding shadow areas can be determined, those are the points with minimal respectively maximal coordinates in the shadowed area. The search area can be limited, considering that an object shadow cannot be aligned to the south and that the minimum zenith angle can be approximated by optional map references (latitude). Figure 4 shows some of the buildings' corners and the corresponding shadow points both marked by crosses.

The apparent disalignment of the buildings' corners is due to an imperfect equalization of the visual image at the altitude edges of the buildings. The visual input image was preprocessed without an underlying height model which leads to the alignment errors. Corresponding corners of buildings and shadows could not be determined for all candidates and even all the matching pairs do not supply the same angles. The reason for this is, that the shadow areas are fuzzy, i.e. shadows are produced by unknown objects or lightened up by reflections of other objects, etc. To calculate the position of the sun we use the average value of all individual measurings, not considered the measured values that are situated outside of the standard deviation.

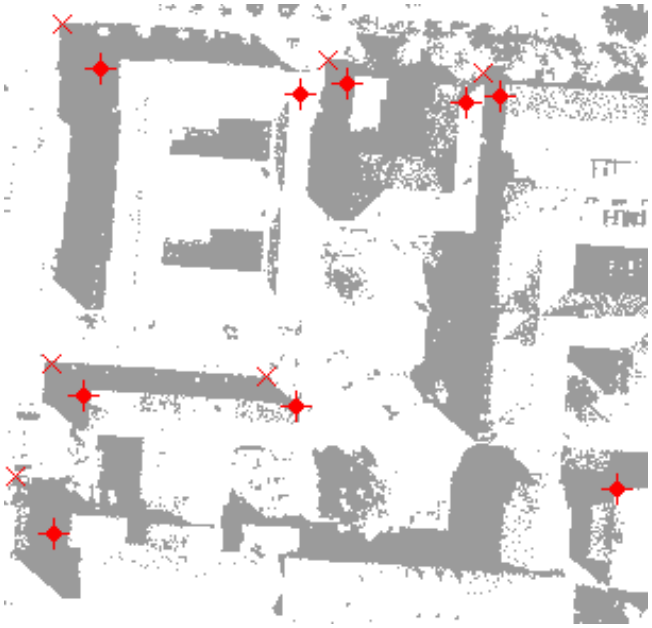

Fig. 4. Shadow image with building and shadow corner

4.2. Projection

With the calculated position of the sun and the height data a *second* shadow image can be produced now. Utilizing a ray tracing procedure it is determined whether a pixel is illuminated by the sun or shaded by other objects. An excerpt of the result data of this procedure together with an overlay of the *first* shadow image is shown in figure 5. The area determined as shadow in both results is drawn in black. The green tone represents areas detected as shadow within the projection only. The brighter grey tone indicates the shadows detected by the application of the luminance threshold.

The most remarkable differences are visible in the wooded areas. This is situated in the fact that the laserscan data recorded in autumn can't reproduce the height of bare trees without leaves. Therefore the projection doesn't produce shadow at the trees' positions. In contrast to this the visual image acquired in summer shows the shadows belonging to the trees. The situation is different at areas with coniferous forest, e.g. in the upper left part of figure 5 where the shadow areas from both results correspond quite well. By exploiting these characteristics it is possible to get evidence for the existence of deciduous trees from analyzing the shadow areas of the data of two laserscan campaigns, one in the summer the other in autumn.

Furthermore there are differences in the two shadow images due to the different acquisition times. For example, the building which can be seen in the laserscan data (figure 6b) is already torn down in the affiliated visual image (figure 6c), which was taken at a later point of time. The differences in the shadow images of this area are shown in

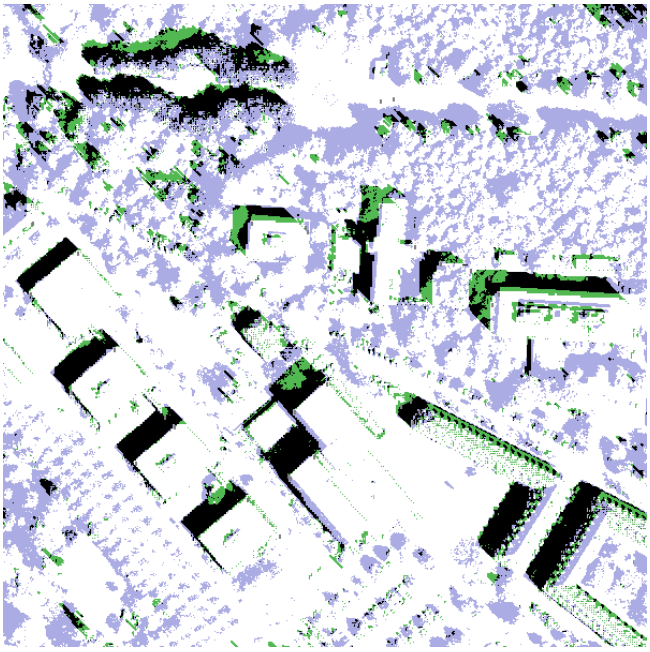

Fig. 5. Shadow result image

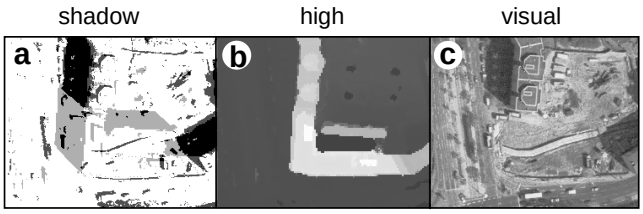

Fig. 6. Demolished building

(figure 6a). Mobile objects such as vehicles or trams also lead to differences in the shadow images.

5. APPLICATION

The radiometric errors to be neutralized by an radiometric equalization can be divided into two groups. On one hand there are hard shadow effects. Those are areas, which cannot be illuminated by the sun, e.g. regions shadowed by high buildings or hills. Another effect emerges from the inclination of the ground. Despite their equal radiometric characteristics areas appear different in the image, depending on the incidence of light and viewing angle. Both aspects have to be considered for a radiometric equalization.

5.1. Inclination image

The inclination of the ground based on the height data is shown in figure 7. The different alignments of the ground are visualized by colour values. Each colour value codes a certain direction presented in figure 8. The roofs of a few rows of houses can be seen.

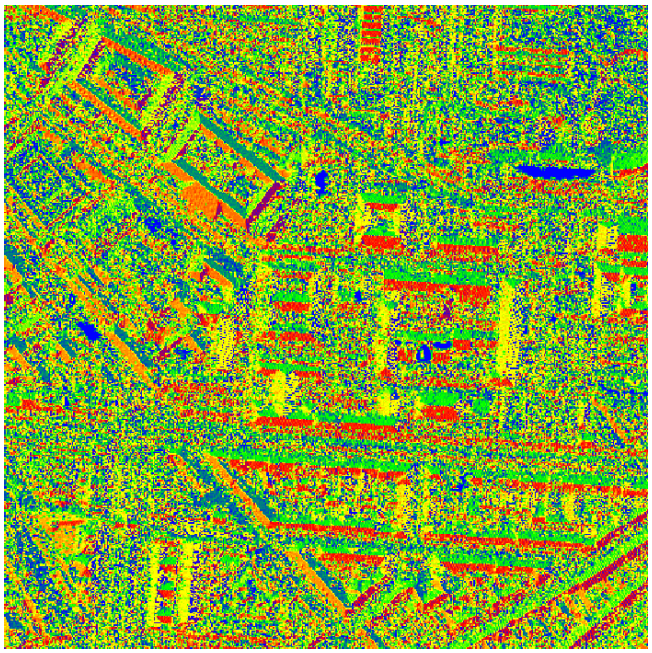

Fig. 7. direction image

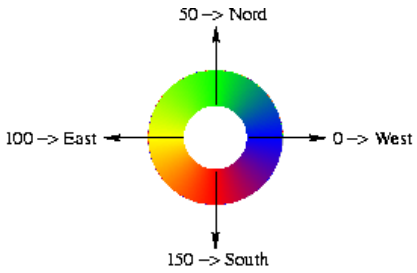

Fig. 8. Meaning of the brightness values

Literature provides several approaches to solve the problem of distortion conditioned by inclination. Itten [Itten, 1993] proposes four methods of equalization based on the model shown in figure 9. The luminance of the inclined surface L_S is calculated from the luminance of a horizontal surface L_H. A statistical, empirical approach supposes a relationship between L_H and L_S from the following relation:

$$L_H = L_S - \cos(i) \cdot m \tag{3}$$

The value m is a measure for the local reflection property. The more intense an object reflects, the larger the value of m gets. Another approach, the cosine correction, calculates L_H according to:

$$L_H = L_S \cdot \frac{\cos(sz)}{\cos(i)} \cdot c \tag{4}$$

The simple variant of the cosine correction sets the variable $c = 1$.

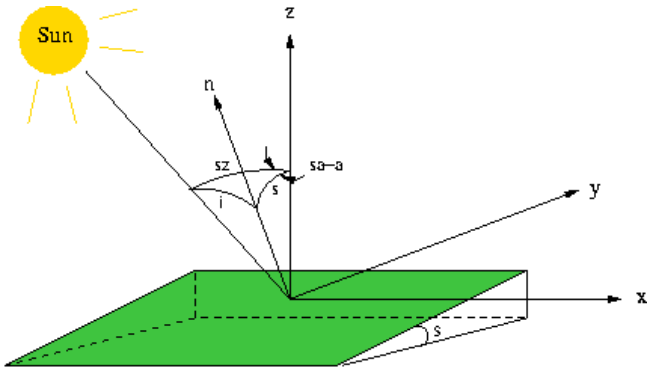

Fig. 9. Derivation of the intermediate angle i from the position of the sun (sz, sa) and the pixel orientation (s, a)

The c-correction approach described in [Itten, 1993] and [Teillet, 1982] will be used here, too. The luminance of the inclined surface is calculated as follows:

$$L_H = L_S \cdot \frac{\cos(sz) + C}{\cos(i) + C} \tag{5}$$

Three directions have to be distinguished in the model shown in figure 9: The direction of the camera, the direction of the sun and the surface normal through the pixel of interest. The zenith angle can be assumed as well known, because the value was estimated in section 4.1. Also the surface normal vector can be determined from the laser scan data. The illumination $\cos(i)$ is calculated from the zenith angle sz, the azimuth angle sa, the inclination of the surface s and the orientation of the surface a:

$$\cos(i) = \cos(sz) \cdot \cos(s) + \sin(sz) \cdot \sin(s) \cdot \cos(sa - a) \tag{6}$$

The correction constant C depends on the material properties of the region of interest and on the type of sensor used to retrieve the data. In [Sandmeier, 1997] values for C for different object classes were reported. The values range from $-0,15$ to $11,74$. Settlements, area of arable land, deciduous, coniferous and mixed forest have C values from $0,25$ to $0,39$. In principle it's possible to empirically determine correction constants C for all object classes for the equalization process. The correction constant used in this approach was set to $C = 0,28$ for the whole settlement area following [Sandmeier, 1997].

5.2. Radiometric Equalization

Regions affected by hard shadow were detected by the procedures described above. For the final equalization a combination of both results is used, but only the regions marked black in figure 5 are taken into account as hard shadow area. Combining the results leads to elimination of the errors seen in the *first* shadow image (the dark regions). On the other hand small differences between the shadow projection and the real shadow area are reduced. The gray values within the hard shadow area have to be increased by a certain $shift$ value. $shift$ is calculated locally for each pixel according to the gradient values of the shadow borders around the buildings which were determined in chapter 3.

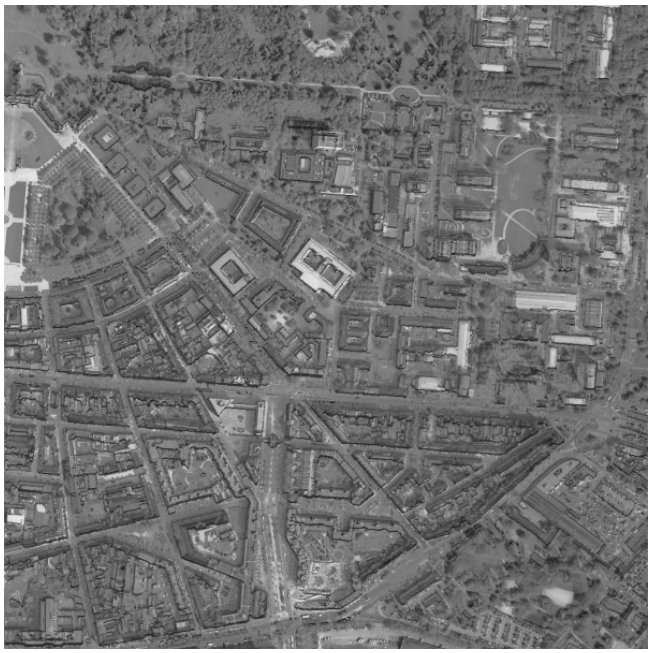

Fig. 10. Radiometric corrected image

The final calculation of the equalized image should take both effects into account. For simplification the quotient appearing in formula 5 is notated as k in the following equations:

$$k = \frac{\cos(sz) + C}{\cos(i) + C} \tag{7}$$

The $shift$ value has to be weighted by the factor k. Using the input image $e(i, j)$ the equalized image $z(i, j)$ computes to:

$$\mathbf{z(i,j)} = \begin{cases} e(i,j) + k \cdot shift & : s(i,j) = 0, \\ e(i,j) + k & : s(i,j) = 255 \end{cases} \tag{8}$$

$s(i, j)$ is the resulting shadow image, the value 0 indicate hard shadow areas. The final equalized image is shown in figure 10. It contains shadow only in those regions with special features (moving objects, temporal changes) as discussed in paragraph 4.2.

6. CONCLUSION

This contribution presented an approach for radiometric equalization of visual remote sensing data using multisensor imagery. For the process the inclination of the terrain towards the sun and observing sensor have been taken into account. Hard shadows were treated seperatly and equalized according to their local features extracted from laserscan data and visual images. The certainty of the shadow detection process was increased by the concurrent evaluation of multisensor data. The contribution closed with a discussion of the results.

7. REFERENCES

[Baumgartner *et al.*, 1999] Baumgartner, A., Eckstein, W., Heipke, C., Hinz, S., Mayer, H., Radig, B., Steger, C., Wiedemann, C. TUM-Research on Road Extraction publisher: Christian Heipke and Helmut Mayer, pp 43-64 1999

[Bückner, 1998] Bückner J. Model Based Road Extraction for the Registration and Interpretation of Remote Sensing Data ISPRS Commission IV Symposium on 'GIS - Between Visions and Applications', Stuttgart, Germany, 7.9.-10.9.98 1998

[Bückner *et al.*, 2000] Bückner J., Pahl M., Stahlhut O. GEOAIDA - A Knowledge Based Automatic Image Data Analyser for Remote Sensing Data CIMA 2001, Second International ICSC Symposium on ADVANCES IN INTELLIGENT DATA ANALYSIS, June 19-22 2001, Bangor, Wales, U.K. 2000

[Itten, 1993] Itten Klaus I., Meyer Peter Geometric and Radiometric Correction of TM Data of Mountainous Forests Areas IEEE Transactions on Geoscience and Remote Sensing, Vol. 31, No. 4, pp. 764-770 1993

[Sandmeier, 1997] Sandmeier Stefan Radiometrische Korrektur des Topographieeffekts in optischen Satellitenbildern Vergleich eines semi-empirischen Verfahrens, mit einem physikalisch-basiertem Modell Photogrammetrie, Fernerkundung, Geoinformation, No. 1, pp. 23-32 1997

[Steinle 1999] Steinle E., Bähr H.-P. Laserscanning for change detection in urban environment Altan & Gründig (eds.): Third Turkish-German Joint Geodetic Days 'Towards A Digital Age', Volume I, pp 147 - 156, Istanbul, Turkey, ISBN 975-561-159-2 (Vol. I) 1999

[Teillet, 1982] Teillet P. M., Guindon B., Goodenough D.G. On the slope-aspect correction of multispectral scanner data Canadien Journal of Remote Sensing, Vol. 8, No. 2, pp. 84-106 1982

[Tönjes *et al.*, 1999] R. Tönjes, S. Growe, J. Bückner and C.-E. Liedtke Knowledge-Based Interpretation of Remote Sensing Images Using Semantic Nets Photogrammetric Engineering and Remote Sensing, Vol. 65, No. 7, pp. 811-821 July 1999